Review of capacitive coupling human body communications based on digital transmission☆

Taewook Kang, Kwang-Il Oh, Hyungil Park, Sungweon Kang*

Intelligent SoC Research Department, ETRI, Daejeon, Republic of Korea

Abstract

Human body communications (HBC) have been studied as an enabling technology to meet the recently increased demands for low-power and high-simplicity in wireless body area networks for wearable-device applications. Previous works on HBC focused mainly on channel modeling with a measurement method, signal transmission scheme, and transceiver implementation. In particular, the digital transmission, invented as a customized approach for the human body channel, has contributed to develop low-complexity HBC systems. This paper addresses on-going research on capacitive coupling HBC based on digital transmission by exploring recent literature.
ⓒ 2016 The Korean Institute of Communications Information Sciences. Publishing Services by Elsevier B.V. This is an open access article under the CC BY-NC-ND license (http://creativecommons.org/licenses/by-nc-nd/4.0/).

Contents

1. Introduction

As essential to use mobile devices such as smart-phones, smart-pads, and smart-watches used in daily life and growing need for sensor network systems for healthcare services, wireless body area networks (WBAN) have become increasingly

important [1,2]. Human body communications (HBC) is considered to be an effective method to realize WBANs to support low-power and low-complexity devices [3]. HBC uses the human body as a transmission channel without wireless or wired connections [4–6]. Simple and intuitive touch allows for the transfer of data and the creation of wireless networks for WBAN devices [3,7]. Previous research including up-to-date results on HBC, can be classified into three parts: channel modeling of the human body with a signal measurement method [8–14], modulation scheme [3,15–19] and frame synchronization [3,17–19] for achieving a desired data rate, and practical implementation of an HBC transceiver [18,20,21].

Human body channel models can be divided into signal transmission methods of capacitive coupling and galvanic coupling [22]. In capacitive coupling, a signal is delivered by forming an electric field induced by the signal electrode [11], and in galvanic coupling, a signal is controlled by an applied current flow considering the human body as a waveguide [23]. This paper addresses only capacitive coupling techniques, which achieve better performance compared to that of galvanic coupling when frequencies higher than 60 kHz are considered for desired data rates supporting WBAN applications [1,22]. Previous literatures show the analysis results of channel properties based on the measured data such as path-loss according to frequency and transmission distance [10,11,13], and time-delay parameters of a channel impulse response [9,12,14] such as root-mean-square (RMS) delay spread and coherence bandwidth. The signal path of the human tissue is also interpreted as electric circuits in [2,11] and electric field equations in [13]. The channel model of IEEE standards 802.15.6 for WBANs describes the impulse response for HBC in terms of the size of the ground planes of the transmitter (Tx) and receiver (Rx) and the distance between the Tx and Rx [8].

While there are various conventional modulation techniques for HBC introduced from the wireless communications such as frequency-shift keying (FSK) [20] and phase-shift keying (PSK) [24], this paper focuses on the digital transmission since the HBC transceiver using the digital transmission can be implemented without a digital-to-analog converter (DAC), an analog-to-digital converter (ADC), or radio frequency (RF) blocks. This reduces the size and power consumption of the device [3]. The frequency selective digital transmission (FSDT), one of the fundamental structures of the digital transmission, has been adopted as an HBC Tx in IEEE standard 802.15.6 for WBANs [3]. Based on the FSDT, the methods for increasing data rates [15–17], improving spectral efficiency [19], and reducing the detection complexity of the length of the Hamming distance (HD) computation [25] were presented in recent approaches. In [3,17–19], preamble structures and frame detection methods are proposed to enhance the synchronization performance for the digital transmission.

Implementation methodology for HBC transceivers has significant influence on the performance of HBC systems. Since HBC is based on the mechanism of the electrical field coupling between a transceiver and the human body, maximizing the coupling effect and minimizing the interference from ambient
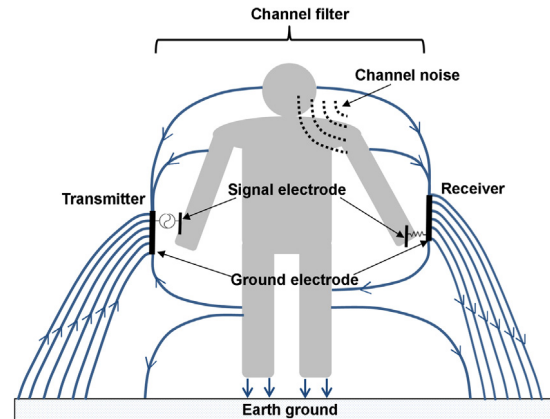

Fig. 1. Channel model of capacitive coupling HBC.

noise are the key factors for the performance improvement [20]. Several schemes for implementation have been suggested, including adaptive frequency hopping FSK [20], direct digital transmission using a Manchester code [7], and digital transmission using Walsh code (WC) [18]. In this paper, the implementation of a transceiver based on the digital transmission is mainly described with the examining specific structural characteristics of the digital blocks and the analog front end (AFE).

Section 2 presents an HBC system model along with the reviews on the channel modeling of the human body. Section 3 deals with the schemes for the data transmission and frame synchronization, in terms of Tx structures, and preamble structures with customized detection methods, respectively. Section 4 describes the implementation designs of HBC transceivers and their essential operating mechanisms. The conclusion is given in Section 5.

2. HBC system model and channel analysis

2.1. HBC system model for digital transmission

Fig. 1 shows a channel model of a capacitive coupling HBC. Capacitive coupling uses a signal electrode for transmission and reception of the signal, with a floating ground electrode, at both sides of the Tx and Rx. The induced signal from the Tx generates an electric potential with the ground electrode coupled to the earth ground. The Rx recognizes the transmitted signal by detecting changes in the electric field. The channel properties are affected by differences in the postures of the human body and surroundings, which behave as conductance variations between the earth ground and return paths [4,22].

If the channel model is considered as signal paths from the Tx and Rx, it can be simplified to a channel filter consisting of the effective paths through the air and on the body [8]. The channel model document for WBANs presents the channel filter as an impulse response in terms of the size of the ground planes of the Tx and Rx and the distance between the Tx and Rx [8]. The channel path loss increases as the size of the ground planes and the distance between the Tx and Rx become smaller and farther, respectively. The interference signals of electromagnetic waves generated from various electronic devices act as channel noise by absorbing
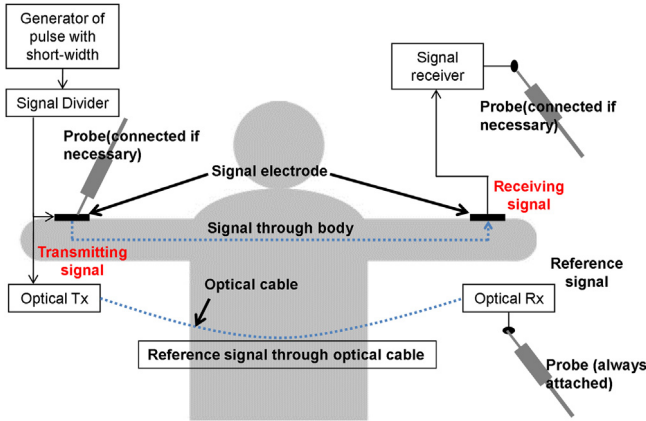
Fig. 2. Measurement setup of impulse response of human body channel.

Fig. 3. Block diagram of FSDT transmitter.

into the human body due to the antenna effects of the human body [26,27]. In [8], the channel noise is shown to have a Gaussian distribution. With consideration of a linear discrete-time channel, the received signal in the digital transmission can be presented as

$$y_k = \sum_{i=0}^{L-1} h_i m_{k-i} + n_k \qquad (1)$$

where y is the output signal, m is the binary input of {0, 1}, n is white Gaussian channel noise, and h is the impulse response of a causal system with L multipath terms for a human body channel.

2.2. Channel measurement

Fig. 2 shows a measurement setup to measure the impulse response of the human body channel [9,14]. The generator module generates a short pulse whose magnitude response is a sinc function crossing the first zero amplitude at the frequency of the reciprocal of the pulse width. The pulse width should be sufficiently narrowed to cover the maximum desired frequency of the channel response. The transmitted pulse signal and received signal passing through the human body are measured at the same time by the transmit trigger signal offered by the optical cable to measure the delay properties. The probe is connected to the measurement equipment through a balun [10,11] or, by using a differential probe [9,14] instead of a passive probe, to isolate grounds between the Rx module and the equipment. If the experiment is interested only in path loss, the Tx transmits a signal containing a single frequency to be measured, and then the Rx measures the amplitude or power of the received signal. Hence, the experimental setup is simplified by removing the devices related to optical signals required measuring the time delay of the received pulse signal.

2.3. Analysis of channel model

Table 1 presents the summary of channel analyses from recently published papers. The measurement data can be divided into two subjects, the impulse response [9,12,14] and the path
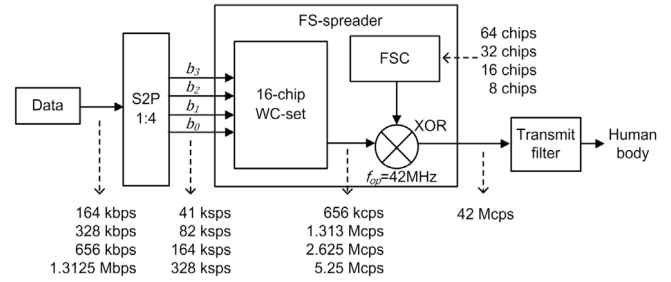
loss [10,11,13]. With the measurement of the impulse response, the channel parameters related to the time delay properties are derived such as mean delay, RMS delay spread, and analysis on the coherence bandwidth. Based on the measurements of path loss in terms of the distance between Tx and Rx, and according to frequency, the human body channel is interpreted as circuit models in [11] and electric field equations composed of near-field and far-field in [13].

The measurement setup, and an analysis based on the measured data of the channel interference are presented in [28]. The power spectral density (PSD) of the effective interference sources is derived after the compensation of measured data with the equivalent circuit model of the input impedance of the human body. Moreover, it shows the simulated bit-error-performance (BER) degradation according to the power of the interference signal.

3. Data transmission and frame synchronization

3.1. Digital data transmission

With the properties of the digital transmission, the center frequency f_c is determined by the half of the operating clock frequency f_{op}, and the data rate increases linearly with an increase in the f_{op} if the length of the symbol-code is fixed. Table 2 presents the comparison of the recent data transmission schemes based on the digital transmission in terms of the transmit scheme, maximum data rate, f_c, and 3 dB bandwidth in accordance with the transmit spectral mask (TSM). The FSDT is standardized in the IEEE standards 802.15.6 for WBAN as a HBC Tx [3]. Fig. 3 shows a block diagram of the FSDT transmitter with a maximum data rate of 1.3125 Mbps using an f_{op} of 42 MHz [3]. The center frequency of the FSDT is determined as 21 MHz considering the regulations of the frequency allocations for WBANs [29]. The information bits enter a serial-to-parallel (S2P) block to yield a 4-bit parallel signal. The 4-bit signal is mapped to one of 16-chip WCs, and spread by using a frequency shift code (FSC) of a [0 1] repeated code in the frequency-selective (FS)-spreader. The spread code, defined as the symbol-code, passes through a transmit filter to be satisfied with the TSM requirements [3]. Based on the basic structure from the FSDT Tx [3], the multi-level baseband coding increases a maximum data rate by combining two WCs into a three-level signal [17]. The direct WC mapping [18], and direct spreading using the FSC without WCs [19] simplify

Table 1
Summary of channel modeling.

Work	Analysis parameters	Frequency (MHz)	Analysis contents
[8]	Modeling of the impulse response	5–50	– Equations for impulse response generation, – Path loss in terms of distance of the Tx and Rx, and the size of ground electrode of the Tx and Rx
[9]	Correlation function and RMS delay spread of the impulse response	0–80	– Measurement setup for measuring the impulse response, – Properties of RMS delay spread of the impulse responses, – Coherence bandwidth analysis
[10]	Path loss	0.1–100	– Gains of signal path in terms of the distance between Tx and Rx, and according to frequency, – Differences of path loss with and without using balun
[11]	Capacitance and path loss	1–100	– Interpretations of the human body channel as circuit models, – Ground coupling capacitance, capacitance between the Tx and Rx electrodes, – Gains of signal path in terms of the distance between Tx and Rx, and according to frequency
[12]	Path loss and time delay properties of the impulse response	5–80	– Path loss and delay properties of the impulse responses based on the measured data from 70 human subjects, – Modeling of the impulse response fitted with a series of random variables
[13]	Electric field equation and path loss	0.1–100	– Interpretation of the signal propagation mechanism using near-field and far-field equations, – Verifying theoretical formulations of path loss with the measured data, – Path loss in terms of the distance between the Tx and Rx, and according to frequency
[14]	Path loss, time delay properties of the impulse response, and modeling of the impulse response	10–100	– Path loss according to frequency, - Delay properties of the impulse response such as coherence bandwidth, mean delay, and RMS delay spread based on the measured data from over 90 human subjects, – Fitting models of the impulse response

Table 2
Digital transmission schemes of HBC.

Work	Transmit scheme	Maximum data rate (Mbps)	f_c (MHz)	3 dB bandwidth (MHz)
[3]	FSDT	1.3125	21	18.375–23.625
[15]	Parallelized multi-spreader	3.9375	21	15.75–26.25
[16]	Parallelized multi-spreader	2.2969	21	18.375–23.625
[17]	Multi-level baseband coding	60	80	n.a.
[18]	Direct Walsh code mapping	2	16	8–22
[19]	Direct spreading using FSC	1.3125	21	20.34375–21.65625

n.a. = data not available.

the Tx structure by excluding the spreading process using an FSC, and the S2P process using a look up table of a WC set, respectively. Fig. 4 shows a block diagram of the digital transmission employing a multi-spreader with a maximum data rate of 3.9375 Mbps using an f_{op} of 42 MHz. The three WC-sets arranged in parallel increase the maximum number of input bit to 12 [15], and these bits are divided into three-bit groups for corresponding WC-sets. The code combiner [16] combines the three-bit streams of WC_1, WC_2 and WC_3 from each WC-set into a single-bit stream SBS as follows:

$$SBS = (WC_1 \text{ and } WC_2) \text{ or } (WC_1 \text{ and } WC_3)$$
$$\text{or } (WC_2 \text{ and } WC_3), \qquad (2)$$

which is equivalent to an output of the carry-out of a binary full adder.

In the Rx, the received signal can be determined as a hard-decision binary value by jointly using comparator and clock and data recovery (CDR) in the AFE [17,18]. Assuming perfect frame synchronization, when the received signal is from the Tx using a single WC-set such as in [3,17–19], a maximum likelihood (ML) detector computes the HD between the hard-decision bit stream from the AFE and all of the candidate symbol-codes, and then finds the candidate symbol-code vector
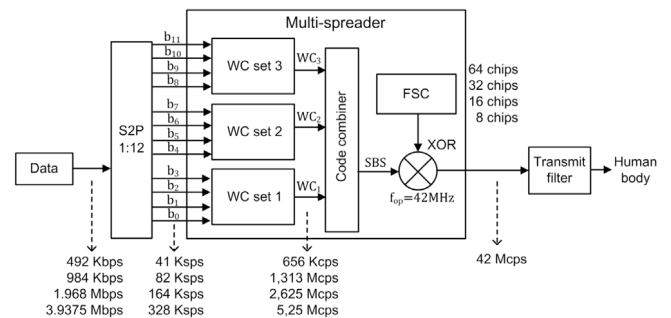
Fig. 4. Block diagram of digital transmission with multi-spreader.

$\hat{\mathbf{c}}$ satisfying

$$\hat{\mathbf{c}} = \arg \min_{c \in S} d(\mathbf{c}, \mathbf{z}) \qquad (3)$$

where, S denotes the set of symbol-code, $d()$ is the HD between two vectors, and $\mathbf{z}$ is the code vector of the hard-decision received signal. In [3,17,18], S is a corresponding subset of the WC, while the S in [19] is composed of an FSC and a bit-inverted FSC. To detect received signal from the Tx with the multi-spreader structure shown in Fig. 4 [15,16], the ML detector is modified to calculate the HD between the decoded

Table 3
Comparison of preamble structures.

Work	Length (chips)	Preamble structure
[3]	2048	[64-bit Gold code × 4 times repetition] × spreading with 8-bit FSC
[17]	128	[32-bit M-sequence] × spreading with 4-bit WC
[18]	256	[128-bit M-sequence] × spreading with Manchester code
[19]	2048	[64-bit M-sequence × 3 times repetition + 64-bit different M-sequence] × spreading with 8-bit FSC

signal of the hard decision bit stream and all of the symbol-codes from each WC-set; it finds the candidate vectors $\hat{\mathbf{c}}_i$ satisfying

$$\hat{\mathbf{c}}_i = \arg\min_{\mathbf{c_i} \in S_i} d\left(\mathbf{c_i}, \mathbf{z}\right) \qquad (4)$$

where $i = 1, 2$, and 3, and S_i denotes each subset of symbol-code vectors from the corresponding WC_i. Then, each $\hat{\mathbf{c}}_i$ is de-mapped to the corresponding ith bit-group. The independent HD calculations for each of the ith WC sets result in a linear increase in the number of HD calculations with an increase in the data rate.

3.2. Frame synchronization

Table 3 lists the recently presented preamble structures for HBC based on the digital transmission. The bandwidth and shape of the PSD of the preamble signal should be identical to those of the transmit data signal to avoid signal distortions by the Tx filter, which is designed to be fit with the frequency response of the data signal. The center frequency and bandwidth of the preamble signal can be shifted by spreading a wide-band random code, such as a gold code or a M-sequence, using an FSC, and adjusted by the ratio of the lengths between the random code and FSC [19]. However, the spreading process generates additional peaks of autocorrelation values neighboring the desired point. The repetition of the same short sub-preambles applied in [3,19] can obtain a repetition diversity gain, but it reduces the margin of the correlation difference between the first highest peak of the desired point and the second highest peak. To overcome these trade-off relations in the performance, detection algorithms depending on the preamble structures are required. The optimum ML detection is infeasible due to its considerable complexity. The autocorrelation values for every chip index are computed and stored to search the chip index of the maximum correlation value, where the correlation is calculated as

$$M(k) \equiv \sum_{i=0}^{D-1} P_i z_{k+i} \qquad (5)$$

where, $M(k)$ is the correlation value at the kth chip index of the time-delay, z is the hard-decision received signal, and P is a preamble with a length of D. The alternative threshold detection reduces the computation complexity by using a threshold value. It detects $M(k)$, higher than the threshold value, as the chip index of the desired point [30]. Threshold detection combined with ML detection [19] improves the detection accuracy compared to that of [30] with the proposed

detection algorithm utilizing the preamble structure, composed of three of the same consecutive sub-preambles followed by a different last sub-preamble.

4. Implementation of HBC transceiver

4.1. Brief introduction of HBC transceiver implementation

Since the communication channel between the Tx and Rx using the human body is different from a wired or wireless communication channel, specialized implementation techniques are required for a successful communication. There have been several efforts of implementation dedicated for the human body communication [7,18,20]. Although each report shows its own remarkable performance and has advantages or disadvantages over the other works, we select two of these implementations in this section. Fig. 5 shows a simplified block diagram of two different implementations of an HBC transceiver. The first implementation is adaptive frequency hopping FSK HBC transceiver and the second is an HBC transceiver using the digital transmission [18,20]. In [20], a frequency hopping technique is introduced to HBC to mitigate the temporally and spatially varying channel loss. According to [21], the 30–120 MHz frequency band shows the highest performance, although there are still several commercially occupied bands such as those for cordless phones, FM radio, and walkie-talkies. By using a frequency-hopping technique, the transceiver continuously examines which frequency band is clean and has low interference from ambient noise in the 30–120 MHz frequency band, and then uses the selected channel for data transmission using the FSK technique. As shown in Fig. 5(a), several RF blocks are required for the frequency-hopping technique with the FSK modulation of the baseband signal. These RF blocks include an FSK modulator, a mixer, and an LNA. These require additional power consumption and die area.

Unlike the design in [20] that uses RF blocks for the frequency-hopping FSK modulation, the digital transmission does not require any RF blocks, leading to simplification of the Tx and Rx structures as shown in Fig. 5(b). The discrete-component implementation of the digital transmission is presented in [18], where every building block of the transceiver for the digital transmission, including AFE block, operates in the baseband domain. Instead of using an FSKmodulator in the Tx and demodulator in the Rx, the HBC transceiver uses the FS-spreader and FS-despreader to acquire a processing gain on the received signal. The rest of this section discusses the implementation of the digital transmission and its advantages over other schemes in terms of its simple implementation.
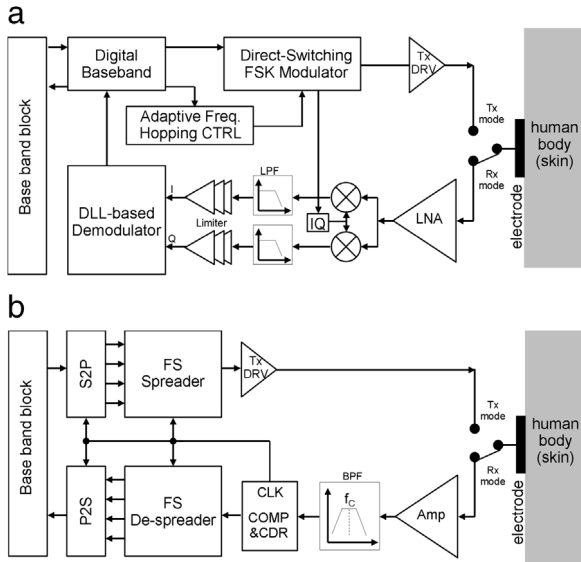
Fig. 5. Simplified block diagram of (a) adaptive frequency hopping FSK HBC transceiver, (b) HBC transceiver with digital transmission.

4.2. Overall architecture of HBC transceiver of digital transmission

Fig. 6 shows an overall block diagram of the transceiver using the digital transmission [18]. This is a fundamental structure for other implementations [3,15–17,19] of the digital transmission presented in the previous section in terms of the bit-to-symbol-code mapping process. The transceiver mainly consists of an HBC Tx, HBC Rx, and AFE. For full duplex communication, time division duplexing (TDD) is adopted in this implementation where the Tx or Rx are operated during their own allocated time slot to share the common transmission channel of the human body. The Tx_EN signal controls the transmitting and receiving time slot by enabling or disabling the Tx driver and AFE.

There are several digital building blocks in the Tx that comprise a transmitting data frame for TDD communication. The transmitting data frame mainly consists of a header, preamble, and baseband data. Since data transmission in the HBC transceiver with the digital transmission is performed in the baseband domain, there is no need for a modulation block such as an FSK modulator. To increase the processing gain on the transmitting data, the FS-spreader block is implemented after the data scrambler. The detailed structure of the FS-spreader is shown in Fig. 6. The original data from baseband block is parallelized by the 1–4 S2P block for mapping an incoming 4-bit code to the specific 64-chip-width WC among 16 WC set. A 4-bit symbol is directly mapped to the 64-chip WC, as shown in the look up table in Fig. 6. Therefore, if the original bit rate of the baseband data is N Mbps, the chip rate at the Tx driver is $N \times 16$ Mcps. The transmitting digital signal is delivered directly to the electrode when TX_EN is "high". Although only the direct WC mapping in Table 2 is depicted in Fig. 6, the FS-spreader using an FSC can be implemented by simply adding the spreader for the FSC [3]. Similarly, if the code combiner [16] is added after the outputs of three parallel
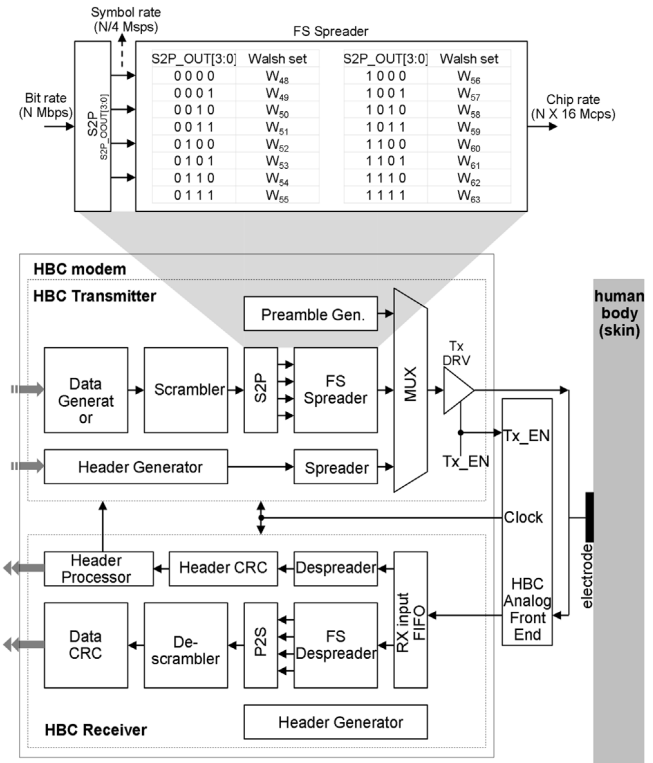

Fig. 6. Overall block diagram of HBC transceiver with FSDT and frequency selective spreader.

WCs, an FSDT transmitter with a multi-spreader can also be implemented.

In the HBC Rx, there are also several digital building blocks and an AFE to successfully recover the transmitted data from the Tx. After recovering the data and clock signal at the AFE, the transmitted frame is de-capsulized with an Rx input FIFO, header cyclic redundancy check (CRC), and header processor. Since the transmitted data are spread using the FS-spreader at the HBC Tx, the received data are delivered to the FS-despreader and parallel-to-serial (P2S) to decode the spread data. The same look up table as that of the Tx is used for correct de-spreading. In accordance with the variations of the FS spreader in the Tx such as the addition of the spreader using FSC [3] or a multi-spreading scheme [15,16], the corresponding counterparts are also equipped in the Rx. After the de-scrambler and data CRC, the original baseband data from HBC Tx is recovered. The transceiver operates only in the baseband domain; it needs no RF component. Therefore, it has enough room to achieve lower power consumption and a small die occupation area, and is less of a burden on the design migration of other fabrication processes.

4.3. AFE design for HBC transceiver for digital transmission

Fig. 7 shows a detailed block diagram of the AFE and CDR of the HBC transceiver using digital transmission. The main operation of the AFE is the recovery of transmitted digital data and clock. Since the Rx uses an independent clock source that typically has a slightly different frequency from that of the Tx, the Rx continuously extracts and tracks the clock information
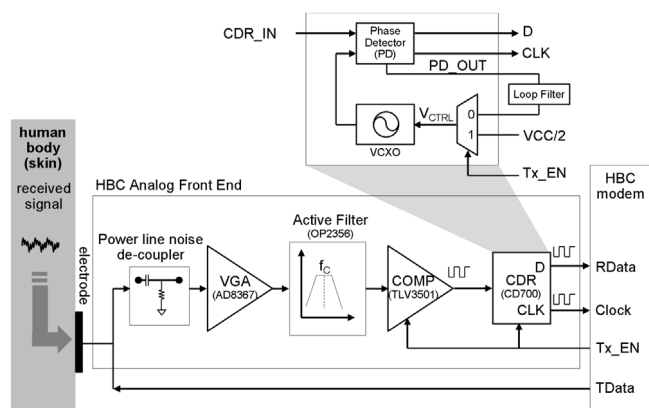
Fig. 7. Block diagram of HBC AFE and CDR.

from the received signal for data processing of the successive digital block. The AFE mainly consists of a low frequency noise de-coupler, variable gain amp (VGA), active filter using an OP-AMP, comparator (COMP), and CDR. To amplify the received small signal and restore the signal level to the logic level for the CDR input, the VGA and COMP are used.

The low frequency noise de-coupler blocks low frequency noises from AC power lines or fluorescent lamps. The amplitudes of these frequencies could be several tens of volts. Owing to the antenna effect of the human body on ambient noises [27], these low frequency and high amplitude noises cause signal saturation for the input of the analog amplifier. A band pass filter located after the VGA effectively filters the residual ambient noises, and extracts the signal component that has the same fundamental frequency as the transmitted signal. Since the fundamental frequency of the signal is determined by the WC set, the cutoff frequency of the band pass filter should be configured to cover the frequency band of the transmitted signal. A Bessel filter with a flat group delay that preserves the shape of the received wave is used in this design to minimize the jitter induced by group delay mismatches. Instead of implementing the band pass filter by cascading a low pass filter and a high pass filter, only a fourth-order active high pass filter with 8 MHz cutoff frequency is implemented using an OP-AMP. The high frequency component can be effectively diminished by selecting the OP-AMP with an appropriate high frequency cutoff bandwidth and manipulating the input hysteresis level of the COMP.

The CDR supplies the clock signal to the Tx and Rx. In transmitting mode when the Tx_EN is "high", the control voltage (V_{CTRL}) for the internal voltage controlled crystal oscillator (VCXO) inside the CDR is set to be VCC/2 to prevent frequency variations during data transmission. In receiving mode when the Tx_EN is "low", however, the V_{CTRL} is determined by the phase comparison result between CDR_IN and the clock from the VCXO. When the clock is lagging compared to the CDR_IN, the V_{CTRL} increases to push the phase of the clock to be faster than the current phase. When the clock is leading compared to the CDR_IN, the V_{CTRL} decreases to pull the phase of the clock to be slower than the current phase. With this mechanism, the clock information is effectively extracted, and the receiver continuously tracks the phases of the received signal.

5. Conclusion

HBC using the human body as a transmission channel offers intuitive and simple connections without complex wiring, or additional antennas for RF signals. While HBC has great potential to be adopted as a leading communication method for WBAN applications such as sensor network devices on the body, studies on the performance enhancement to secure communication stability regardless of the channel variations due to the different body postures and environments, and low-complexity implementation should be performed previously. Among various methods for realizing a HBC system, capacitive coupling achieves better performance than galvanic coupling in a high frequency band for a high data rate, and long distance transmission. In addition, the digital transmission, a customized transmission method for HBC, lowers the implementation complexity without using an ADC, DAC, or RF related blocks. This paper presented a review of on-going research into capacitive coupling HBCs using the digital transmission in terms of channel modeling, methods for data transmission and frame synchronization, and the implementation methodology of the HBC transceiver.

References

[1] M. Abolhasan, J. Lipman, D. Smith, A. Jamalipour, Wireless body area networks: a survey, IEEE Commun. Surv. Tutor. 16 (3) (2014) third quarter.

[2] M. Seyedi, B. Kibret, D.T.H. Lai, M. Faulkner, A survey on intrabody communications for body area network applications, IEEE Trans. Biomed. Eng. 60 (8) (2013) 2067–2079.

[3] IEEE Standard for local and metropolitan area networks—Part 15.6: Wireless Body Area Networks, IEEE 802.15 working group for WPAN, 2012.

[4] T.G. Zimmerman, Personal area networks: Near-field intrabody communication, IBM Syst. J. 35 (3–4) (1996) 609–617.

[5] T.G. Zimmerman, Applying electric field sensing to human–computer-interfaces, in: Proc. CHI, 1995, pp. 280–287.

[6] E. Rehmi Post, Matt Reynolds, Matthew Gray, Joe Paradiso, Neil Gershenfeld, Intrabody buses for data and power, in: The first International Symposium on Wearable Computers 1997. Digest of Papers, 1997, pp. 52–55.

[7] C.H. Hyoung, J.B. Sung, J.H. Hwang, J.K. Kim, D.G. Park, S.W. Kang, A novel system for intrabody communication touch-and-play, in: IEEE Int. Symp. on Circuit and Systems, Kos, Greece, May 2006, pp. 1343–1346.

[8] Channel Model for Body Area Network (BAN), IEEE P802.15-08-0780-12-0006, Nov. 2010.

[9] T.W. Kang, J.H. Hwang, C.H. Hyoung, I.G. Lim, H.I. Park, S.W. Kang, Performance evaluation of human body communication system for IEEE 802.15 on the effect of human body channel, in: Proc. IEEE ISCE, Jun. 2011, pp. 232–235.

[10] Z. Lucev, I. Krois, M. Cifrek, A capacitive intrabody communication channel from 100 kHz to 100 MHz, IEEE Trans. Instrum. Meas. 61 (12) (2012) 3280–3289.

[11] M.D. Pereira, G.A. Alvarez-Botero, F.R. de Sousa, Characterization and modeling of the capacitive HBC channel, IEEE Trans. Instrum. Meas. 64 (10) (2015) 2626–2635.

[12] J.H. Hwang, T.W. Kang, S.O. Park, Y.T. Kim, Empirical channel model for human body communication, IEEE Antennas Wirel. Propag. Lett. 14 (2015) 694–697.

[13] J. Bae, K. Song, H. Lee, H. Cho, H.-J. Yoo, The signal transmission mechanism on the surface of human body for body channel communication, IEEE Trans. Microw. Theory Tech. 60 (3) (2012) 582–593.

[14] J.H. Hwang, T.W. Kang, Y.T. Kim, S.O. Park, Measurement of transmission properties of HBC channel and its impulse response model, IEEE Trans. Instrum. Meas. 65 (1) (2016) 177–188.

[15] T.W. Kang, I.G. Lim, J.H. Hwang, C.H. Hyoung, H.I. Park, S.W. Kang, A method of increasing data rate for human body communication system for body area network applications, in: IEEE Veh. Technol. Conf., Sep. 2012, pp. 1–5.

[16] T.W. Kang, I.G. Lim, K.H. Park, S.W. Kang, S.E. Kim, Improving data rate in the human body communications, in: 2014 International Conf. on Information and Communication Technology Convergence, ICTC, Oct. 2014, pp. 51–52.

[17] Ch.K. Ho, J.H. Cheong, J.H. Lee, V.V. Kulkarni, P. Li, X. Liu, M.K. Je, High bandwidth efficiency and low power consumption Walsh code implementation methods for body channel communication, IEEE Trans. Microw. Theory Tech. 62 (9) (2014) 1867–1878.

[18] C.H. Hyoung, S.W. Kang, S.O. Park, Y.T. Kim, Transceiver for human body communication using frequency selective digital transmission, ETRI J. 34 (2) (2012) 216–225.

[19] T.W. Kang, J.H. Hwang, S.E. Kim, K.I. Oh, H.I. Park, I.G. Lim, S.W. Kang, Highly simplified and bandwidth-efficient human body communications based on IEEE 802.15.6 WBANs standard, ETRI J. (2016) 1074–1084. early access. http://dx.doi.org/10.4218/etrij.16.2716.0003.

[20] N. Cho, L. Yan, J. Bae, H.-J. Yoo, A 60 kbs–10 Mbs adaptive frequency hopping transceiver for interference-resilient body channel communication, J. Solid-State Circuits 44 (3) (2009) 708–717.

[21] N. Cho, J. Yoo, S.-J. Song, J. Lee, S. Jeon, H.-J. Yoo, The human body characteristics as a signal transmission medium for intrabody communication, Trans. Microw. Theory Tech. 55 (5) (2007) 1080–1086.

[22] M.A. Callejon, D. Naranjo-Hernandez, J. Reina-Tosina, L.M. Roa, A comprehensive study into intrabody communication measurements, IEEE Trans. Instrum. Meas. 62 (9) (2013) 2446–2455.

[23] M. Amparo Callej´on, J. Reina-Tosina, D. Naranjo-Hern´andez, L.M. Roa, Measurement issues in Galvanic intrabody communication: Influence of experimental setup, IEEE Trans. Biomed. Eng. 62 (11) (2015) 2724–2732.

[24] R. Xu, N.W. Chiu, H. Zhu, S. Hengying, J. Yuan, Equation environment coupling and interference on the electric-field intrabody communication channel, IEEE Trans. Biomed. Eng. 59 (7) (2012) 2051–2059.

[25] T.W. Kang, I.G. Lim, J.H. Hwang, S.E. Kim, S.W. Kang, K.H. Park, S.W. Son, A complexity-efficiency human body communications, in: IEEE Asia-Pacific Conf. Commun., Denpasaar, Indonesia, Aug. 29–31, 2013, pp. 445–446.

[26] J.H. Hwang, T.W. Kang, Y.T. Kim, S.O. Park, Analysis on co-channel Interference of human body communication supporting IEEE 802.15.6 BAN standard, ETRI J. 37 (3) (2015) 439–449.

[27] J.H. Hwang, C.H. Hyoung, K.H. Park, Y.T. Kim, Energy harvesting from ambient electromagnetic wave using human body as antenna, Electron. Lett. 49 (2013) 149–151.

[28] J.H. Hwang, T.W. Kang, J.H. Kwon, S.O. Park, Effect of electromagnetic interference on human body communication, IEEE Trans. Electromagn. Compat. 59 (1) (2017) 48–57.

[29] Supplemental Information for HBC, IEEE 802.15-10-0318-00-0006, May. 2010.

[30] H.K. Choi, S.Y. Hwang, J.R. Lee, Communication apparatus and method using pseudo-random code, US Patent 13/696,740, filed May. 7, 2010.